N88-23738

BOUNDARY-LAYER STABILITY AND AIRFOIL DESIGN*

Jeffrey K. Viken
ESCON
Grafton, Virginia 23692

SUMMARY

Several different natural laminar flow (NLF) airfoils have been analyzed for stability of the laminar boundary layer using linear stability codes. The NLF airfoils analyzed come from three different design conditions: incompressible, compressible with no sweep, and compressible with sweep. Some of the design problems are discussed, concentrating on those problems associated with keeping the boundary layer laminar. Also, there is a discussion on how a linear stability analysis was effectively used to improve the design for some of the airfoils.

INTRODUCTION

The problem of designing an airfoil to perform well over a range of conditions instead of just one point is a significant one and is well appreciated by anyone associated with airfoil design. In many cases an airfoil has been chosen for its high-lift characteristics even though it has a high profile drag at cruise. Presently, performance gains associated with low cruise profile drags are being emphasized. The challenge here is to design an airfoil to perform well at cruise while retaining good high-lift performance.

A key element in the design of low-drag laminar flow airfoils is linear stability theory which offers a quantitative method of examining the growth of disturbances in the laminar boundary layer. This tool allows the airfoil designer to design the airfoil for the desired amount of laminar foil. In addition, by designing the laminar boundary layer with just enough stability for the desired conditions, the compromises with other performance areas of the airfoil can be minimized.

This paper uses linear stability theory to illustrate some of the problems associated with designing an airfoil for extensive laminar flow and emphasizes the problems at the cruise condition. Laminar boundary-layer stability analysis is conducted on airfoils for three different design conditions: incompressible, compressible with no sweep, and compressible with sweep. The specific design considerations associated with each flying condition are discussed.

---

*Research by the author was supported by the National Aeronautics and Space Administration under NASA Contract No. NAS1-17670.

SYMBOLS

A/A_o	amplitude ratio of disturbance from initial point of instability
c	chord length
c_d	profile drag coefficient
c_ℓ	section lift coefficient (listed in figures as CL)
c_m	section pitching moment coefficient about the quarter chord point (listed in figures as CMC/4)
C_p	pressure coefficient, $(p - p_\infty)/q_\infty$
f	disturbance frequency, Hz
M	free-stream Mach number
n	logarithmic amplification, $n = \ln(A/A_o)$
p	static pressure
q	dynamic pressure, $\rho U^2/2$
R	chord Reynolds number, $\rho_\infty U_\infty c/\mu_\infty$
s	surface distance
t/c	thickness ratio of airfoil, thickness/chord (listed in figures as T/C)
u'	perturbation velocity in the x direction
U	potential flow velocity in the x direction
x,y	two-dimensional Cartesian coordinate axes
α	angle of attack, deg (listed in figures as ALP)
δ_f	trailing-edge flap deflection in degrees (+: up) (listed in figures as DELTA F)
Λ	wing sweep, deg (listed in figures as SW)
λ	wavelength
ρ	mass density
ψ	wave angle of perturbation vortices with respect to potential flow direction, deg

Subscripts:

max	maximum value
∞	free-stream conditions

Other:

CF	crossflow
LFC	laminar flow control
LS	lower surface
NLF	natural laminar flow
TS	Tollmien-Schlichting
US	upper surface
DESB159	airfoil designation
DESB165	airfoil designation
NLF(1)-0414F	airfoil designation
HSNLF(1)-0313	airfoil designation
SAL8EYO	airfoil designation

LINEAR STABILITY THEORY

Free-stream turbulence, vibrating boundaries, sound from the propulsion system, or surface roughness may introduce disturbances into the laminar boundary layer which can be amplified. At present, there is no quantitative analysis for calculating a given amplitude of disturbance generated by a given flow environment. Fortunately, because there are such large amplifications of disturbances in the laminar boundary layer before transition, we are still able to give a reasonably good prediction of the transition location. This transition prediction method examines the degree of amplification of a disturbance from the initial point of instability using a linearized form of the Navier-Stokes equations. Linear theory represents a good approximation when the perturbations are weak because the nonlinear stress terms are negligible as compared to those driving the mean flow. The disturbance is assumed to be harmonic and monochromatic. When the flow is essentially two-dimensional, the selectivity of the allowable amplified disturbances dampens all but a narrow range of frequencies which makes the monochromatic assumption reasonable. But seldom are these disturbance waves propagated naturally in a periodic fashion. A more realistic model is a modulated wave packet. Gaster (ref. 1) states that these modulated waves will break down the ordered laminar boundary layer at a lower growth rate than a periodic wave would. The reason he gives is that nonlinear stresses induced by the modulated wave are very much different from those created in the periodic wave train. Naturally, if prediction is to be improved, this aspect must be taken into account.

For two-dimensional airfoils (no sweep), only Tollmien-Schlichting (TS) type disturbances occur. However, on wings with sweep, an instability due to spanwise flow also arises. This problem was discovered by Gray but was illustrated by Dagenhart (ref. 2) when he analyzed the temporal amplification rate versus orientation angle at a specific chord location on a swept airfoil. He showed that there was a sharp peak in the amplification at

approximately 90° relative to the local potential flow. Also there was another broad amplification region with a maximum in the direction of the local potential flow. Thus, the boundary-layer stability problem on a swept wing can be broken up into two parts according to wave orientation. Disturbance waves with $\psi = 0^{\circ}$ travel in the local potential flow direction, while those with an orientation angle within a few degrees of $\psi = 90^{\circ}$ progress nearly normal to the potential flow direction. The former, which are associated with the tangential boundary layer, are often referred to as TS waves since they are similar to the two-dimensional waves studied by Tollmien and Schlichting. The latter are generally called crossflow disturbances since they are associated with the crossflow boundary layer. These disturbances arise from the three-dimensional character of the boundary layer on a swept wing. They are not present in two-dimensional flows. Pfenninger (ref. 3) notes that this separation of the stability problem into two independent parts is physically acceptable as long as strongly amplified crossflow and TS waves do not occur simultaneously. Raetz (refs. 4 to 6), Reed (refs. 7 and 8), and Saric and Yeates (ref. 9) have shown that relatively weak oblique TS waves can distort and stretch streamwise vortices such as crossflow disturbance vortices to produce rapid, resonance like amplification and transition. For this reason, the mutual interaction of amplified disturbances of the two types should be avoided. This mutual interaction can be minimized when highly amplified TS and crossflow disturbances do not occur simultaneously.

According to Rayleigh and Tollmien (ref. 10), boundary-layer profiles without a point of inflection, i.e., $\partial^2 u/\partial y^2 = 0$, are stable with respect to boundary-layer perturbations when viscosity is neglected. Profiles with an inflection point are dynamically highly unstable, even in frictionless flow. The presence of viscosity introduces a relatively mild frictional type of instability to convex boundary-layer profiles without inflection points. This is illustrated in reference 10, page 443, where curves of neutral stability, for both frictional and inflectional instabilities, are shown on plots of nondimensional disturbance wave number versus the Reynolds number based on boundary-layer thickness. The region of amplified wave numbers is much smaller for frictional instabilities than for inflectional instabilities. The band of unstable wave numbers goes to zero as the Reynolds number based on boundary-layer thickness approaches infinity for frictional instabilities, but remains wide for inflectional instabilities. For TS disturbances, accelerating pressure gradients, $dp/dx < 0$, are termed favorable because they result in velocity profiles without inflection points. The more steep the accelerating gradient, the more the relatively mild frictional instabilities are stabilized. For TS disturbances, decelerating pressure gradients, $dp/dx > 0$, are termed adverse because they result in velocity profiles with inflection points. With respect to crossflow disturbances, the spanwise velocity profiles resulting from wing sweep always have inflection points and are always dynamically highly unstable. The steeper the pressure gradient, accelerating or decelerating, the more unstable the crossflow disturbances.

For incompressible TS instabilities, the SALLY analysis code (refs. 11 to 13) is used to calculate disturbance amplification. This utilizes Chebychev polynomials to find the eigenvalues of the incompressible Orr-Sommerfeld equation. A range of frequencies is analyzed for chordwise disturbance growth, and transition prediction is made from the most unstable frequency. A wave orientation angle of $\psi = 0^{\circ}$ is assumed because Squire (ref. 14) has shown that this is the maximum amplified orientation angle in incompressible flow.

For compressible TS disturbances, the COSAL analysis code (ref. 15) is used to calculate the growth of unstable waves. This code utilizes a finite difference scheme to solve the compressible Orr-Sommerfeld equation. For these cases, a range of frequencies is also analyzed and transition predictions are made on the most unstable frequency. However, in compressible flow $\psi = 0^{o}$ is not the most unstable orientation angle of disturbance. A maximization procedure in the COSAL program is used to find the orientation angle-wavelength combination of the most unstable disturbance at each computation station. The density change in compressible flow makes the boundary layer more stable with respect to TS disturbances. Roughly, a rule of thumb is that through a compressible analysis ($M_{local} \approx 1$), one will get the same disturbance amplification at twice as high a chord Reynolds number as in the corresponding incompressible analysis.

Only an incompressible crossflow analysis is made for this paper. The MARIA code (ref. 2), developed from Pfenninger's ideas using Brown's curves (ref. 3), is used to calculate crossflow disturbance amplification. This code incorporates an algorithm to approximate crossflow disturbance amplification from amplification rate solution charts generated from the SALLY code for ten typical crossflow velocity profiles. A range of wavelengths is analyzed and transition predictions are made on the most unstable wavelength. This analysis is the fixed wavelength method and assumes the disturbance is a stationary wave (f = 0). There are some experimental data which seem to indicate that the crossflow vortices are standing vortices on the wing and that the wavelength does not change along the chord. However, there are also data which indicate that the wavelength of the crossflow vortices increases in the chordwise direction with some vortices eventually disappearing. Neither set of data is conclusive to define the actual state of the disturbances at the present time. Compressibility favorably affects crossflow disturbance growth but not as radically as in the case of TS disturbances. For crossflow disturbance amplifications which are calculated with a compressible analysis, the growth in n_{max} will be approximately 10 percent less than the calculated incompressible value.

ANALYSIS OF EXPERIMENTAL RESULTS

An analysis was made of an existing flight experiment to correlate linear stability theory with predicting the transition process for uninteracted TS disturbances. The analysis is of flight tests made on a smooth NACA 66_{2x}-216 airfoil on a King Cobra World War II airplane (refs. 16 to 18). This airfoil section was designed for approximately 60 percent to 65 percent chord laminar flow on both surfaces. Three experimental pressure distributions were analyzed with the incompressible SALLY stability code for TS amplification. They were first published in reference 19, but a typical one is shown here for comparison.

The case shown here was for the upper surface at $c_{\ell} = 0.38$, $M = 0.269$, and $R = 12 \times 10^{6}$ (fig. 1). The pressure distribution is characterized by a leading-edge negative-pressure peak with a local deceleration of 11 percent q_{max}, followed by a very flat negative pressure gradient up to 60 percent chord. The most amplified frequency is 2000 Hz which reaches a logarithmic amplification of $n = 22.958$. This gives a total amplification of $A/A_{o} = 9.344 \times 10^{9}$ up to the point of laminar separation. The chord was 6.2 ft and the free-stream velocity was 280 ft/sec. In free flight, as verified by Gray and Fullam (ref. 17), transition occured at or very close after the point of laminar separation ($x/c = 0.625$). Care must be

taken when extrapolating this result to other cases. There is a strong amplification along the chord for all the frequencies analyzed, but the logarithmic amplification stays under n = 13 up to the 45 percent chord station. The TS disturbances then amplify much quicker in the slight deceleration region from x/c = 0.45 to 0.60. If these strong amplifications occurred further upstream in the chord, then the disturbances could become three-dimensional. Once these TS disturbances become three-dimensional, they grow much quicker than the linear theory predicts (refs. 20 to 23).

Another point that should be noted is that the transition location was considerably different in the wind tunnel than in free flight. For the same pressure distribution, in the wind tunnel with a turbulence level of u'/U = 0.07 percent, transition occurred downstream of the leading-edge negative-pressure peak at x/c = 0.15. Based on this and McCready's results (ref. 24), apparently the scale of atmospheric turbulence in atmospheric boundary layers or jetstream shear layers is so much larger than the microscale turbulence of even the best low turbulence wind tunnels, it is shifted into the region of viscous dissipation. As a result, atmospheric microscale turbulence generally appears too weak to affect transition.

To correlate crossflow disturbance amplification with transition one can look at an experiment of a Northrop modified NACA 66-012 LFC wing swept 30°. Using Brown's theoretical results, Pfenninger calculated total logarithmic amplifications of n = 6 to 8 up to s/c = 0.60 and transition had not yet occurred (ref. 3). Also, transition experiments of J. Carlson on a 15 percent thick, 33° swept nonsuction wing gave transition values of logarithmic amplification at fully developed turbulent flow of n = 12 (ref. 25).

LOW-SPEED (INCOMPRESSIBLE) AIRFOILS

When designing NLF airfoils, there are certain compromises one has to live with, and it is important to maximize the benefits and minimize the losses. When designing for low cruise profile drags, the first thing to be concerned with is the amount of laminar flow desired. This means starting the main pressure rise after that point on each surface. To get extensive laminar flow, for the high Reynolds applications considered in this paper ($R \approx 10 \times 10^6$), a favorable pressure gradient, i.e., accelerated flow, must be designed up to the point of desired transition. For low Reynolds number airfoils it might even be desirable to design a slightly adverse gradient over most of the airfoil. Favorable gradients stabilize the laminar boundary layer with respect to TS disturbance waves, while adverse pressure gradients give velocity profiles with inflection points which are dynamically highly unstable.

As the design Reynolds number increases, more acceleration needs to be designed into the airfoil on each surface to keep the boundary layer laminar up the desired point of transition. To get more acceleration, the airfoil has to be designed thicker overall or with a thinner leading edge, since the pressure gradient in subsonic flow responds inversely with thickness increase. Making the airfoil thicker makes the far aft pressure recovery on the upper surface more critical with respect to separation. Up to a certain point, making the leading edge thinner increases the low drag c_ℓ range at low angles of attack, but increases the chance of laminar separation at the leading edge at high angles of attack. The real problem arises if the leading edge is so sharp that after leading-edge laminar separation the turbulent boundary layer does not reattach to the airfoil. Ideally, the way to design the

airfoil is to design as little acceleration into the airfoil as is needed. This helps alleviate the problems in the rear pressure recovery region and helps the designer to get a thicker leading edge for better $c_{\ell_{max}}$ performance.

Airfoil DESB159 (fig. 2), first published in reference 19, was designed using this philosophy and linear stability theory. Based on the logarithmic TS growths up to transition on the King Cobra flight experiment and other wind tunnel experiments, DESB159 was designed using linear theory with enough acceleration to give the desired amplification at the design point, $c_\ell = 0.454$, $M = 0.4$, and $R = 10 \times 10^6$. The negative pressure gradients on both surfaces are much flatter than for most other NLF airfoils previously designed for use at such a high chord Reynolds number.

The results of the stability analysis for the upper surface of DESB159 at the design point are shown in figure 3. The maximum amplified TS disturbance is f = 3500 Hz which reaches a logarithmic amplification of n = 10.917 at the laminar separation point (x/c = 0.70). The chord used in the analysis was 4.0 ft and the free-stream velocity was 414.7 ft/sec. The analyzed TS frequencies do not even become unstable until x/c = 0.17. This is well below the TS amplification calculated in the King Cobra stability analysis, but the airfoil was designed to also get 70 percent chord NLF in a wind tunnel test where the free-stream turbulence unfavorably affects transition. Also, with some margin of stability, one can expect a range of lift coefficients with low drag in flight instead of only a point design.

The lower surface of DESB159 had similar TS amplification at the design point $c_\ell = 0.454$, $M = 0.4$, and $R = 10 \times 10^6$. The maximum amplified frequency was 2750 Hz, which had a maximum logarithmic amplification of n = 9.214 up to the laminar separation point.

An illustration of the TS amplification, caused by the dynamically highly unstable profiles with inflection points in decelerating flow, is shown in figure 4. This is a plot of the stability analysis of the upper surface of DESB159 at $c_\ell = 0.75$, $M = 0.4$, and $R = 10 \times 10^6$. The flow is decelerated from x/c = 0.15 to the laminar separation point of x/c = 0.70. The maximum logarithmic amplification is doubled from that of the design case. The most unstable analyzed frequency was 3375 Hz, which had a logarithmic amplification of n = 20.715. The chord was 4.0 ft and the free-stream velocity was 414.7 ft/sec. This amplification is comparable with that analyzed in the King Cobra experiments. In free flight, on a smooth wing at $c_\ell = 0.75$, $M = 0.4$, and $R = 10 \times 10^6$, transition might be expected at the laminar separation point for this condition. However, the TS disturbances grow to higher values earlier in the chord than in the King Cobra analysis so it is possible that the disturbances could become three-dimensional sooner.

Because of the problems a thin leading edge gave with respect to $c_{\ell_{max}}$ performance in the design of DESB159, an investigation was conducted to examine the effects on low drag that resulted from thickening the leading edge. Thickness was superimposed directly onto the leading edge region of DESB159, changing as little of the rest of the airfoil as possible. The modified airfoil, DESB165, is shown in figure 5, where the change in surface contour from that of DESB159 is plotted. A comparison of the inviscid pressure distributions of both airfoils is shown in figure 6 at $c_\ell = 0.45$ and $M = 0.4$. The flow accelerates quicker in

the leading-edge region of DESB165 than in that of the original airfoil, DESB159. There is a flat spot in the pressure distribution from x/c = 0.10 to 0.15 and then the flow again accelerates quicker than that of DESB159, merging into the same pressure distribution at about x/c = 0.50. Stability analysis on this design pressure distribution of DESB165 led to an interesting result. It was found that at the design condition of $c_\ell = 0.45$, $R = 10 \times 10^6$, and M = 0.4, this modification to the upper surface resulted in a drop in the maximum TS amplification by approximately a factor of 2.5. This result can be deduced from the stability analysis of the upper surface of DESB165 at the design condition in figure 7. The maximum amplified disturbance frequency is 3500 Hz, which reaches a maximum logarithmic amplification of 9.931 at the laminar separation point. The chord was 4.0 ft and the free-stream velocity was 414.7 ft/sec. The maximum amplified disturbance frequency for DESB159 had a logarithmic amplification of n = 10.917. It appears that the acceleration on DESB165 is tailored such that it is concentrated in the correct place to curb the disturbances near the lower branch of the neutral stability curve where they are small, before they have a chance to multiply. Acceleration is wasted if it is used before the disturbances have begun to amplify (ref. 26).

It was known, however, that the thick leading edge of DESB165 would reduce the c_ℓ range with low drag by causing leading-edge negative-pressure peaks sooner than that of DESB159. This can be seen in figure 8, where the inviscid pressure distributions of DESB159 and DESB165 are plotted at M = 0.4 and $c_\ell = 0.75$. On DESB165, there is a leading-edge deceleration of $0.15q_{max}$ up to x/c = 0.15, whereas the DESB159 airfoil has a slightly negative gradient up to this point. This leading-edge deceleration gives dynamically highly unstable profiles which will give much greater TS amplifications than those of DESB159 up to x/c = 0.15.

The c_ℓ range with low drag can be increased with the use of a small-chord simple trailing-edge cruise flap that can be deflected both positively and negatively for different flying conditions (ref. 27). This small-chord simple flap trades lift due to angle of attack for lift due to flap deflection. As a result, the stagnation point can be kept near the leading edge for different lift coefficients to keep the gradients favorable on both surfaces. This is illustrated in experimental results from NLF(1)-0414F shown in figure 9. NLF(1)-0414F is a derivative of the DESB165 airfoil that is an attempt to distribute the acceleration on the upper surface after the flat region over a wider distance. The results of the wind tunnel experiment of NLF(1)-0414F conducted in NASA Langley's LTPT are published in reference 28. Figure 9(a) shows the pressure distribution and section characteristics at a section lift coefficient of approximately 0.8, $R = 10 \times 10^6$, and M = 0.12 for 0° and 12.5° deflections of the 12.5 percent chord cruise flap. No stability analysis has been conducted on these pressure distributions, but the measured profile drag coefficients show the merit of the cruise flap. With a 0° flap deflection the airfoil needs $\alpha = 3.12^\circ$ to get $c_\ell = 0.837$. The airfoil has a leading edge C_p of -1.85 on the upper surface and the flow decelerates continuously to the trailing edge. The corresponding profile drag coefficient is 0.0084. With the cruise flap deflected 12.5°, the airfoil can get a c_ℓ of 0.794 at $\alpha = -1.99^\circ$. In this case, the upper surface is accelerated continuously up to the main pressure rise at x/c = 0.70. The lower surface is accelerated continuously up to x/c = 0.40, with a slight deceleration from x/c = 0.40 to 0.70, the start of the main pressure rise. The profile drag coefficient at this condition is 0.0032. With the 12.5° flap deflection and the restored favorable gradient, the

profile drag is only 38 percent that of the airfoil at approximately the same c_ℓ with no flap deflection. This reduction in profile drag can also be seen at the cruise lift coefficients with a negative flap deflection. The pressure distributions and section characteristics of NLF(1)-0414F at a section lift coefficient of approximately 0.22 ($M = 0.12$ and $R = 10 \times 10^6$) are shown in figure 9(b) for 0° and -5.0° flap deflections. To get down to $c_\ell = 0.236$ with 0° flap deflection, an angle of attack of -2.44° is needed. At this condition there is a leading-edge negative-pressure peak on the lower surface with a local deceleration of 12.4 percent q_{max}. The profile drag coefficient is 0.0041. With a flap deflection of -5.0° the angle of attack can be increased to -0.46° to get $c_\ell = 0.22$. The flow is now accelerated on both surfaces back to the main pressure rise. The profile drag coefficient at $c_\ell = 0.22$, $M = 0.12$, and $R = 10 \times 10^6$ is now 0.0027. This is only 66 percent that of the drag with 0° flap deflection at approximately the same lift coefficient.

A linear stability analysis was conducted for the upper surface of NLF(1)-0414F at the design condition ($c_\ell = 0.45$, $M = 0.12$, and $R = 10 \times 10^6$) to correlate transition measurements with linear TS amplification. The results of this linear stability analysis are shown in figure 10(a). The maximum amplified disturbance frequency is 1400 Hz, which reaches a maximum logarithmic amplification of $n = 12.636$ at the laminar separation point ($x/c = 0.70$). The chord used was 3.0 ft with a free-stream velocity of 121.9 ft/sec. These disturbance growths are very similar to those calculated for the theoretical pressure distribution of the DESB165 airfoil. Transition measurements were made on the experimental model with surface-mounted hot-film gauges. The gauges were placed at x/c's of 0.50, 0.55, 0.60, 0.65, and 0.70. At the design condition the flow over the gauge at 65 percent chord was fully laminar, and the gauge at 70 percent chord had about 50 percent laminar and 50 percent turbulent flow. This would give a logarithmic amplification up to the beginning of transition of about $n = 11$ to 12. A summary plot of n_{max} against frequency is shown in figure 10(b), which illustrates the highly selective process of the laminar boundary layer with respect to the frequency of TS amplification. Only a small range of frequencies from the total spectrum are highly amplified. Remember, this is a logarithmic plot. If actual values were plotted, the selectiveness would seem more dramatic.

HIGH-SPEED (COMPRESSIBLE) AIRFOILS - NO SWEEP

When increasing the Mach number on an airfoil, one must be alert for additional design considerations due to the effects of compressibility. Compressibility has favorable effects with respect to TS instability. The flow is more accelerated around the airfoil which reduces the TS amplification. With no sweep, the added acceleration does not contribute to any crossflow instability. Also, for a given pressure distribution, the change in density in the boundary layer associated with compressibility helps stabilize the flow with respect to TS disturbances.

The problems with compressibility in airfoil design come mainly in decelerating the flow. With this added acceleration the rear pressure recovery becomes steeper and is more prone to separation than in the low-speed case. Also, one has to be careful that the flow does not over-accelerate around the airfoil and develop into a shock. At these high speeds, an airfoil needs to be designed with less camber than in the incompressible case. An illustration of what happens to an incompressible airfoil at high speeds is shown in figure 11.

This is an inviscid pressure distribution of NLF(1)-0414F at M = 0.70 and $\alpha = -0.953^{o}$. The upper surface has accelerated strongly and becomes supersonic at x/c = 0.20. The accelerated region terminates in a strong shock at x/c = 0.70. This airfoil has too much camber for compressible applications. Camber can be taken out over the whole extent of the airfoil or it can be taken out at the trailing edge with a simple flap deflection. Taking out overall camber of the airfoil makes it better transonically but can hurt low speed performance. Taking out camber with a trailing-edge flap still leaves camber in the airfoil for low speed performance, but causes relatively strongly accelerated flow over the airfoil which leads to shocks sooner at higher Mach numbers.

HSNLF(1)-0313 (fig. 12) is a modified version of NLF(1)-0414F. Camber has been taken out of the trailing edge with a flap deflection of -5.24^{o} (12.5 percent chord flap). Also, the beginning of the pressure rise on the upper surface is moved ahead to x/c = 0.57 to help alleviate the problems of turbulent separation in the pressure recovery region. The inviscid pressure distribution of HSNLF(1)-0313 is also shown in figure 12 at M = 0.70 and c_{ℓ} = 0.26. For this condition, the flow on the upper surface is only slightly supersonic from x/c = 0.34 to 0.58.

The results of the compressible TS stability analysis for HSNLF(1)-0313 are shown in figure 13 at the design point: M = 0.70, c_{ℓ} = 0.26, and R = 10 x 10^{6}. On the upper surface, figure 13(a), the maximum amplified frequency was f = 5000 Hz, which reached a maximum logarithmic amplification of n = 1.688 at the point of laminar separation. The chord used was 4.0 ft and the free-stream velocity was 711.1 ft/sec. On the lower surface of HSNLF(1)-0313 at the design point, figure 13(b), the maximum amplified frequency, f = 5000 Hz, reached a maximum logarithmic amplification of n = 2.937 at x/c = 0.53. The disturbance was stable from x/c = 0.53 to 0.67, the laminar separation point. The lower surface pressure distribution is characterized by a leading-edge deceleration of 2.1 percent q_{max} followed by a strong acceleration up to the laminar separation point. For all the frequencies analyzed, this leading-edge negative-pressure peak does not seem to influence the TS instability.

With such a small TS disturbance amplification at the design chord Reynolds number, chord Reynolds numbers of 15, 20, and 40 x 10^{6} were analyzed on the design pressure distribution of both surfaces. In figure 14(a), the chordwise compressible TS disturbance amplification for the upper surface of HSNLF(1)-0313 at c_{ℓ} = 0.26, M = 0.70, and R = 40 x 10^{6} is shown. The chord is 4.0 ft and the free-stream velocity is 711.1 ft/sec. The maximum amplified disturbance frequency is f = 8000 Hz, which reaches a maximum amplification of only n = 5.357 at the laminar separation point. The stabilizing effects of compressibility and the strong acceleration give very low TS amplification even at this high chord Reynolds number. To illustrate the stabilizing effects of compressibility, the chordwise TS amplification calculated at the same conditions with incompressible stability computations is shown in figure 14(b). The incompressible calculations predict a naximum logarithmic amplification of n = 14.036 up to the laminar separation point. This is a maximum logarithmic amplification that is 2.6 times that calculated in the compressible calculations or a total amplification (A/A_{o}) of 5,878 times greater. The compressible and incompressible chordwise TS disturbance amplification of the lower surface of HSNLF(1)-0313 is shown in figures 15(a) and 15(b), respectively. The maximum compressible logarithmic amplification

was n = 9.793 at f = 8000 Hz. This disturbance became stable at x/c = 0.51 and remained stable up to the laminar separation point at x/c = 0.67.

HIGH-SPEED (COMPRESSIBLE) AIRFOILS - WITH SWEEP

When designing for high cruise Mach numbers, one is inevitably led to designing wings with sweep to keep down the maximum local Mach numbers on the surface. The same benefits and problems arise from compressibility as in the non-swept case; however, with sweep another boundary-layer instability arises from the spanwise flow across the wing. The strong acceleration that stabilizes the boundary layer with respect to TS disturbances leads to crossflow instabilities. For the most part, at high Mach numbers and with any significant sweep, one has to design around the problem of crossflow instability.

The first example of linear stability analysis of a swept wing in compressible flow is the analysis of a flight condition of the NASA glove for the F-14 in the Variable Sweep Transition Flight Experiment. This glove was designed by Waggoner, Campbell, and Phillips (National Transonic Facility, Transonic Aerodynamics Division, NASA Langley). The case shown here is at M = 0.70 and at an altitude of 20,000 ft. This analysis was done at the mid-semispan location with the wing leading edge swept 20° and the trailing edge swept 2.5°. The chord here was 8.75 ft and the free-stream velocity was 711.1 ft/sec, which gave a chord Reynolds number of 24.15×10^{6}. The upper surface pressure distribution used in the stability calculation is a theoretical three-dimensional calculation with viscous effects calculated using the TAWFIVE computer code (ref. 29).

The results of the compressible chordwise logarithmic TS amplification for the F-14 NASA glove calculated by the COSAL program are shown in figure 16. For the analyzed frequencies, the maximum logarithmic amplification is n = 8.74 for a frequency of 4000 Hz. In this case, there is a significant amount of the total amplification after the pressure minimum, when the boundary-layer profiles have inflection points. For the maximum amplified frequency of 4000 Hz, there is a logarithmic amplification of n = 4.0 up to the laminar separation point. The linear TS amplification (uninteracted) is much weaker than that needed to cause transition, but there is a crossflow instability caused by the spanwise flow. The calculated crossflow instability for this case, using the incompressible MARIA code (ref. 2), is shown in figure 17. The most unstable nondimensional wavelength of disturbance, $\lambda/c = 0.0012$, grows to maximum logarithmic amplification of n = 9.497 at x/c = 0.46, decaying slightly up to the laminar separation point at x/c = 0.50. However, smaller wavelengths get amplified to significant values early in the chord. For a nondimensional wavelength of $\lambda/c = 0.0008$, an n of 8 is exceeded at x/c = 0.16. The maximum compressible TS logarithmic amplification at x/c = 0.16 is n = 1.4, for the frequencies analyzed. In this case, one can expect transition after x/c = 0.16 to be solely due to crossflow instability, with essentially no TS interaction. Given that this incompressible calculation could overpredict compressible crossflow amplification by 10 percent, crossflow instability might not cause transition until $x/c \approx 0.30$.

Another high-speed airfoil analyzed was SAL8EYO. The two-dimensional inviscid pressure distribution is shown in figure 18. At the design condition, $c_{\ell} = 0.20$ and M = 0.75, there is slightly accelerated flow over the upper surface back to x/c = 0.60. The lower

surface is strongly accelerated back to x/c = 0.55 with a slight deceleration from x/c = 0.55 to 0.60. The main pressure recoveries for both surfaces start at the x/c = 0.60 location. There is a very shallow supersonic zone on the upper surface extending from x/c = 0.10 to 0.60. The design philosophy behind this type of airfoil is that with the flat pressure gradient on the upper surface, one can get a higher design Mach number before shocks start to develop. Also, on most airfoils, the pressure rise on the upper surface is much greater than that on the lower surface. With SAL8EYO, the decelerations on both surfaces are much more equal, thereby somewhat alleviating the problems of turbulent separation on the upper surface. Note that both these pressure recoveries have to be refined. The turbulent boundary layer separates in both recoveries when the flow is fully turbulent at the design condition. This airfoil is included to provide an example of problems associated with boundary-layer stability.

The compressible chordwise TS amplification for the upper surface of SAL8EYO at M = 0.75, c_ℓ = 0.20, and R = 10 x 10^6 is shown in figure 19. For all the SAL8EYO and CBLXF2 cases, the chord is 4.0 ft and the free-stream velocity is 788.3 ft/sec. The maximum amplified disturbance frequency is 5000 Hz, which reaches a maximum logarithmic TS amplification of n = 7.365 up to the laminar separation point. This logarithmic growth is still well below transitional levels. The incompressible logarithmic crossflow amplification for the upper surface of SAL8EYO is shown in figure 20. In this case, the analyzed pressure distribution has been transformed applying simple sweep theory to an infinitely swept untapered wing. The wing sweep used, $\Lambda = 20^\circ$, gave a free-stream Mach number of 0.798 and a chord Reynolds number of 10.64 x 10^6, with the same normal Mach number of 0.75. Note that the pressure distribution shown in the plot is still the two-dimensional inviscid pressure distribution. This is the case for all the pressure distributions shown with SAL8EYO and CBLXF2. The maximum amplified wavelength is λ/c = 0.0006, which reaches a maximum logarithmic amplification of only n = 1.644 at x/c = 0.035 decaying to n = 0.0 at x/c = 0.10. The crossflow amplification here is essentially insignificant. For this case on the upper surface, realizing that the TS amplification will be somewhat greater when analyzed at $\Lambda = 20^\circ$, transition should not occur before the laminar separation point at x/c = 0.60.

The compressible chordwise logarithmic TS amplification for the lower surface of SAL8EYO at M = 0.75, c_ℓ = 0.20, and R = 10 x 10^6 is shown in figure 21. For all the frequencies analyzed, the only amplification that occurs is in the slight deceleration region from the pressure minimum (x/c = 0.55) up to the laminar separation point at x/c = 0.60. The maximum amplified disturbance is at a frequency of 5000 Hz and has a logarithmic amplification of only n = 2.517. The incompressible chordwise crossflow amplification, with 20° of sweep (no taper) for the lower surface of SAL8EYO, is shown in figure 22. At a free-stream Mach number of 0.798 and R = 10.64 x 10^6, the maximum amplified wavelength is λ/c = 0.0024, which reaches a maximum logarithmic amplification of n = 9.798 at the laminar separation point. Because of the stabilizing effects of compressibility, transition would probably occur between x/c = 0.50 and 0.60.

With swept wings at higher Reynolds numbers, this crossflow instability on the lower surface becomes more of a problem and dominates the transition process. This is illustrated in figure 23, where the incompressible chordwise crossflow instability for the lower surface

of SAL8EYO at $R = 15.96 \times 10^6$ is shown. Simple sweep theory was again used to transform the two-dimensional inviscid pressure distribution at $M = 0.75$ into the analyzed pressure distribution on a 20° swept, non-tapered wing at $M = 0.798$. The maximum amplified wavelength is $\lambda/c = 0.0020$, which reaches a maximum logarithmic amplification of $n = 13.604$ at the laminar separation point. For this case, the uninteracted crossflow disturbances can be expected to cause transition between $x/c = 0.20$ and 0.30.

To try and relieve this problem, a new longer surface pressure distribution was sketched and analyzed. This pressure distribution is shown in figure 24, along with the incompressible chordwise crossflow amplification. The pressure distribution is much flatter overall, and the total crossflow amplification is reduced considerably. The maximum logarithmic amplification is $n = 8.157$ ($\lambda/c = 0.0020$) up to the laminar separation point. Uninteracted, this crossflow disturbance amplification should not cause transition. However, with this reduced overall acceleration, the TS amplification is greater than in the SAL8EYO case. This is illustrated in figure 25, where the same CBLXF2 pressure distribution is analyzed for chordwise compressible TS disturbance growth. The maximum amplified disturbance ($f = 5000$ Hz) now has a logarithmic amplification of $n = 7.684$ up to the laminar separation point. There will probably be some interaction between the crossflow vortices and the TS disturbances from $x/c = 0.50$ to $x/c = 0.64$, and transition might occur before the laminar separation point.

CONCLUSIONS

1. When designing an airfoil for extensive NLF, linear stability theory gives a quantitative analysis of disturbance growth in the laminar boundary layer that empirical transition predictions miss. Linear stability theory allows the tailoring of the airfoil for specific design conditions, minimizing the off-design compromises.

2. In view of the King Cobra flight results (NACA 66_{2x}-216), where uninteracted linear TS logarithmic amplifications were in excess of $n = 20$, it appears that TS disturbance amplifications can rise to much higher levels than are commonly expected, before transition occurs. These much higher disturbance amplifications can be gained from the much lower free-stream disturbances encountered in flight than in even the best low turbulence wind tunnels. This is provided that there are no acoustic disturbances generated by the airplane in the highly amplified TS frequency range.

3. The negative pressure gradient should be tailored so that acceleration is concentrated near the lower branch of the neutral stability curve of the most amplified TS disturbance. The concentrated acceleration curbs the disturbances when they are small, before they have had a chance to grow, and results in much lower maximum TS amplifications than when acceleration is wasted in a stable region or when the acceleration is used after the disturbances have grown to a high level.

4. When designing an NLF airfoil with a relatively thick leading edge for favorable high-lift performance, the use of a cruise flap is necessary to increase the low-drag range of the airfoil. For different c_ℓ values, favorable gradients can be maintained on both surfaces by keeping the stagnation point at the leading edge and varying the deflection of the cruise flap.

5. As the Mach number increases, compressibility stabilizes the laminar boundary layer and also gives more acceleration on the airfoil. As long as there is no sweep, the main design problem changes from obtaining laminar flow to designing against shock formation and turbulent separation in the pressure recoveries.

6. For swept wings at high Mach numbers, the crossflow instability in the laminar boundary layer seems to be the major deciding factor in determining the amount of laminar flow, especially on the lower surface.

REFERENCES

1. Gaster, M.: Propagation of Linear Wave Packets in Laminar Boundary Layers. AIAA Journal, Vol. 19, No. 4, April 1981, pp. 419-423.

2. Dagenhart, J. Ray: Amplified Crossflow Disturbances in the Laminar Boundary Layer on Swept Wings with Suction. NASA TP-1902, November 1981.

3. Pfenninger, Werner: Laminar Flow Control Laminarization. Special Course on Concepts for Drag Reduction, AGARD-R-654, June 1977, pp. 3-1 thru 3-75.

4. Raetz, G. S.: A New Theory of the Cause of Transition in Fluid Flows, Northrop Norair Report NOR 59-383 (BLC-121), June 1959.

5. Raetz, G. S.: "Current Status of Resonance Theory of Transition," Summary of Boundary Layer Control Research, ASD-TDR-63-554, Part I, Chapter A, March 1964.

6. Raetz, G. S.: "Calculation of Precise Proper Solutions for the Resonance Theory of Transition," Theoretical Investigations Task 3.3, AFFDL-TR-64-185, Part I, December 1964.

7. Reed, H. L.: Wave Interactions in Swept Wing Flows. AIAA Paper No. 84-1678, 1984.

8. Reed, H. L.: Disturbance Wave Interactions in Flows with Crossflow. AIAA Paper No. 85-0494, 1985.

9. Saric, W. S.; and Yeates, L. G.: Experiments on the Stability of Crossflow Vortices in Swept Wing Flows. AIAA Paper No. 85-0493, 1985.

10. Schlichting, Herman (J. Kestin, transl.): Boundary-Layer Theory. New York: McGraw-Hill Book Co., Sixth Edition, 1968.

11. Srokowski, Andrew J.; and Orszag, Steven A.: Mass Flow Requirements for LFC Wing Design. AIAA Paper No. 77-1222, 1977.

12. Orszag, Steven A.: Accurate Solution of the Orr-Sommerfeld Stability Equation. Journal of Fluid Mech., Vol. 50, Part 4, 1971, pp. 689-703.

13. Srokowski, Andrew J.: SALLY User's Guide. LAR-12556. Available through COSMIC, 112 Barrow Hall, The University of Georgia, Athens, Ga. 30602, 1979.

14. Squire, H. B.: On the Stability of Three-Dimensional Distribution of Viscous Fluid Between Parallel Walls. Proc. Roy. Soc. London A142, pp. 621-628, 1933.

15. Malik, Mujeeb R.: COSAL--A Black Box Compressible Stability Analysis Code for Transition Prediction in Three-Dimensional Boundary Layers. NASA CR-165925, May 1982.

16. Gray, W. E.: Transition in Flight on a Laminar-Flow Wing of Low Waviness (King Cobra). R.A.E. Report No. 2364, March 1950.

17. Gray, W.E.; and Fullam, P. W. J.: Comparison of Flight and Wind Tunnel Measurements of Transition on a Highly Finished Wing (King Cobra). R.A.E. Report No. 2383, June 1950.

18. Smith, F.; and Higton, D. J.: Flight Tests on "King Cobra" F.Z.440 to Investigate the Practical Requirements for the Achievement of Low Profile Drag Coefficients on a "Low Drag" Aerofoil. R.A.E. Report No. 2078, A.R.C. 9043, August 1945.

19. Viken, Jeffrey K.: Aerodynamic Considerations and Theoretical Results for a High Reynolds Number NLF Airfoil. Master's Thesis, George Washington University, January 1983.

20. Schubauer, G. B.; and Klebanoff, P. S.: Contributions on the Mechanics of Boundary Layer Transition. NACA Rep. 1289, 1956.

21. Saric, W. S.; Kozlov, V. V.; and Levchenko, V. Y.: Forced and Unforced Subharmonic Resonance in Boundary Layer Transition. AIAA Paper No. 84-0007, 1984.

22. Saric, W. S.; and Thomas, A. S. W.: Experiments on the Subharmonic Route to Turbulence in the Boundary Layer. Turbulence and Chaotic Phenomena in Fluids. Edited by Tatusmi, North Holland, 1984.

23. Reynolds, G. A.; and Saric, W. S.: Experiments on the Stability of a Flat Plate Boundary Layer with Suction. AIAA Paper No. 82-1026, 1982.

24. McCready, P.: Turbulence Measurements by Sailplane. Journal of Geophysical Research, vol. 67, no. 3, pp. 1041-1050, 1962.

25. Carlson, J. C.: Results of a Low Speed Wind-Tunnel Test to Investigate the Influence of Leading Edge Radius and Angle of Attack on the Spanwise Spread of Turbulence Along the Leading Edge of a Sweptback Wing. Northrop Report NOR-64-30, 1964.

26. Reed, H. L.; and Nayfeh, A. H.: Stability of Flow Over Plates with Porous Suction Strips. AIAA Paper No. 81-1280, 1981.

27. Pfenninger, W.: Investigations on Reductions of Friction on Wings in Particular by Means of Boundary Layer Suction. NACA Technical Memorandum 1181, August 1947.

28. McGhee, Robert J.; Viken, Jeffrey K.; Pfenninger, Werner; Beasley, William D.; and Harvey, William D.: Experimental Results for a Flapped NLF Airfoil with High Lift/Drag Ratio. NASA TM-85788, May 1984.

29. Melson, N.D.; and Street, C.L.: TAWFIVE: A User's Guide. NASA TM-84619, September 1983.

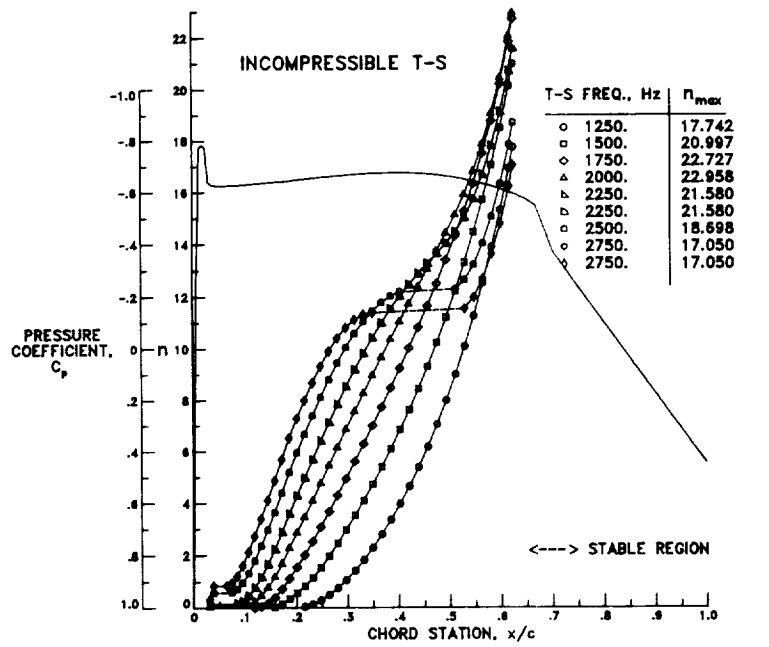

Figure 1.- Pressure distribution and the incompressible logarithmic amplification of various TS disturbance frequencies of Gray and Fullam's experiments on an NACA 66_{2x}-216 airfoil.

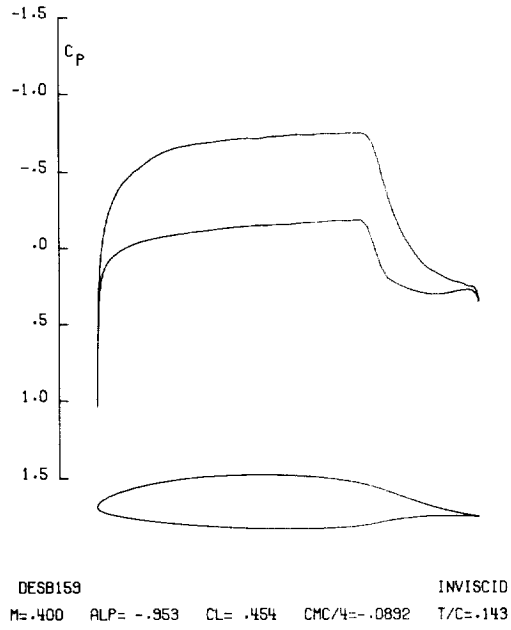

Figure 2.- Calculated inviscid pressure distribution of DESB159 at the design case.

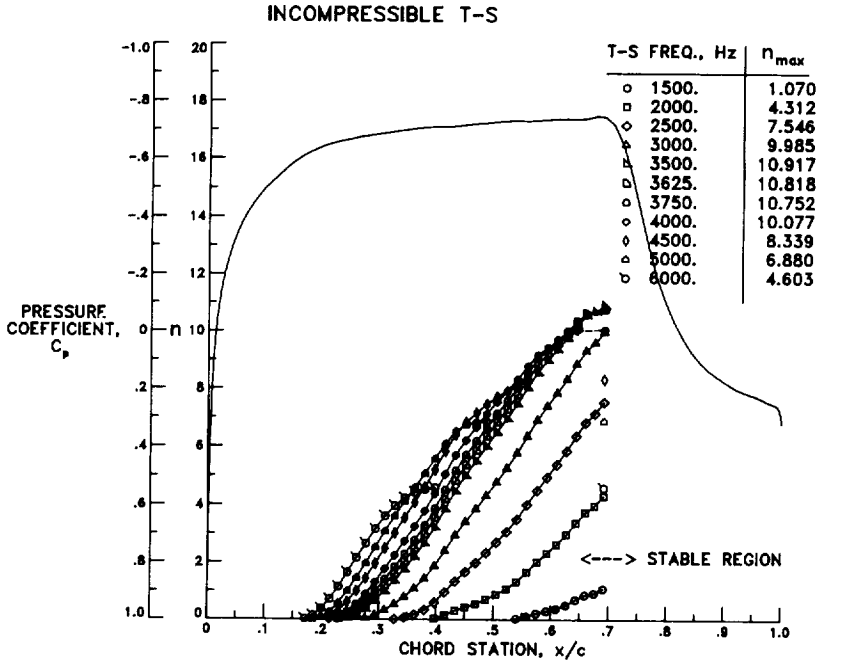

Figure 3.- Calculated pressure distribution and the incompressible logarithmic amplification of various TS disturbance frequencies for the upper surface of DESB159 at design.

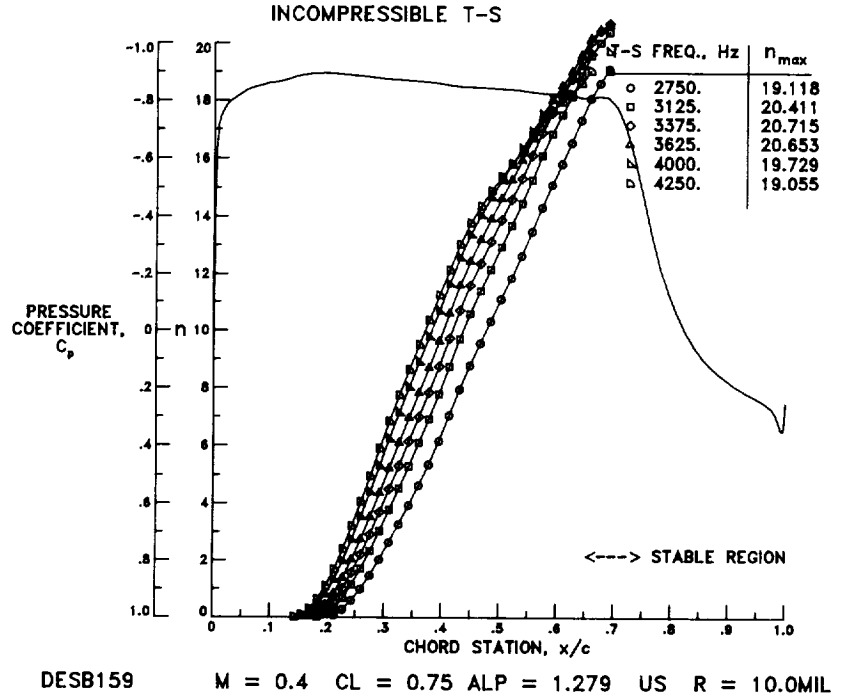

Figure 4.- Calculated pressure distribution and the incompressible logarithmic amplification of various TS disturbance frequencies for the upper surface of DESB159 at climb conditions.

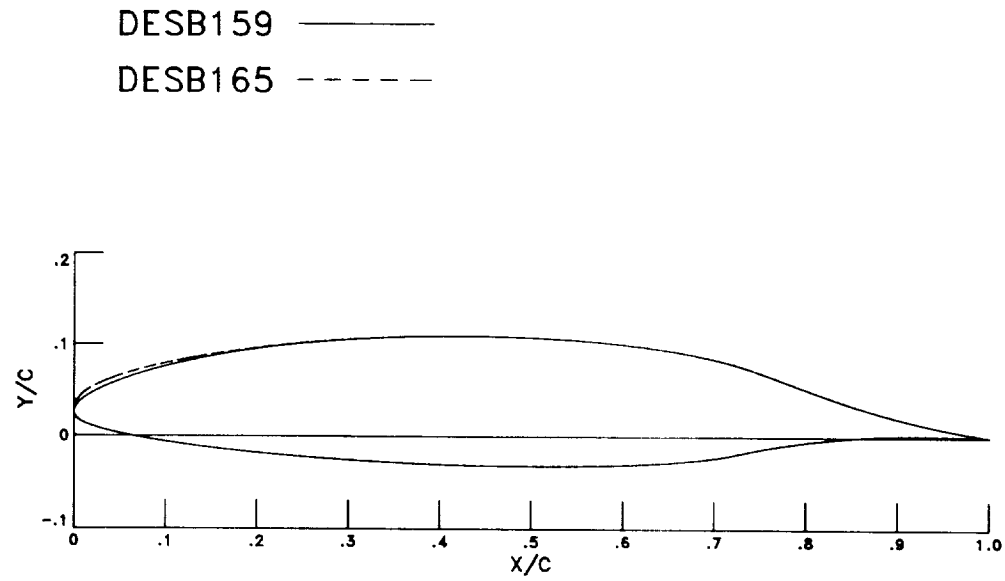

Figure 5.- Comparison of airfoil profile DESB165 with the baseline profile DESB159.

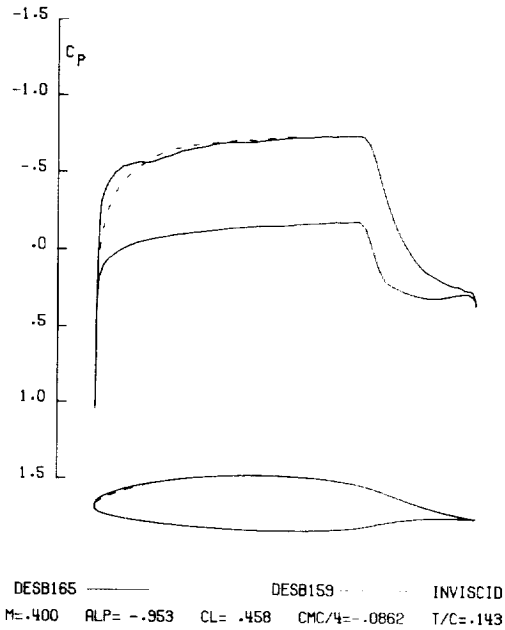

Figure 6.- Comparison of inviscid pressure distributions of DESB165 airfoil with the DESB159 airfoil at the design condition.

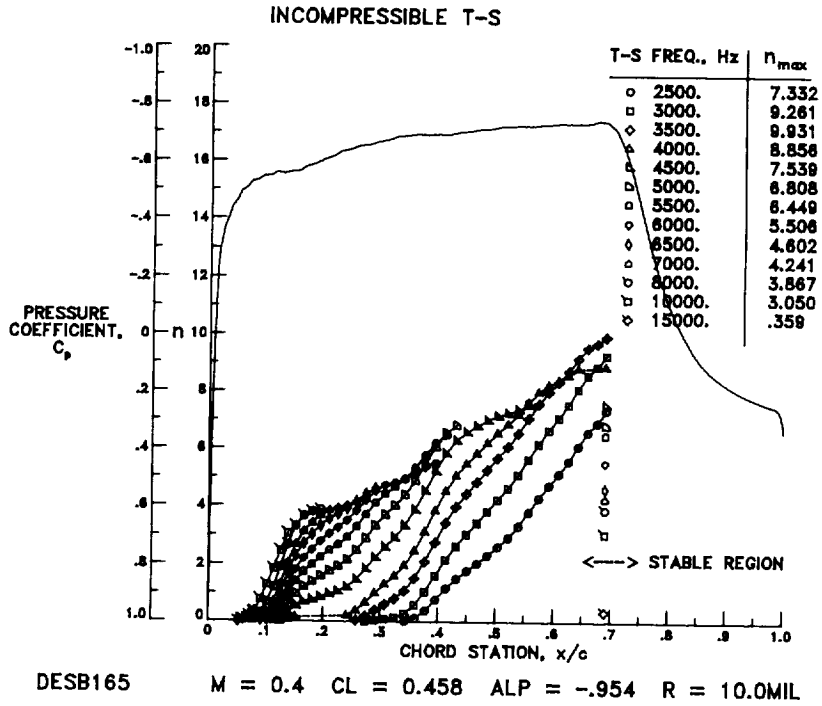

Figure 7.- Calculated pressure distribution and the incompressible logarithmic amplification of various TS disturbance frequencies for the upper surface of DESB165 at design.

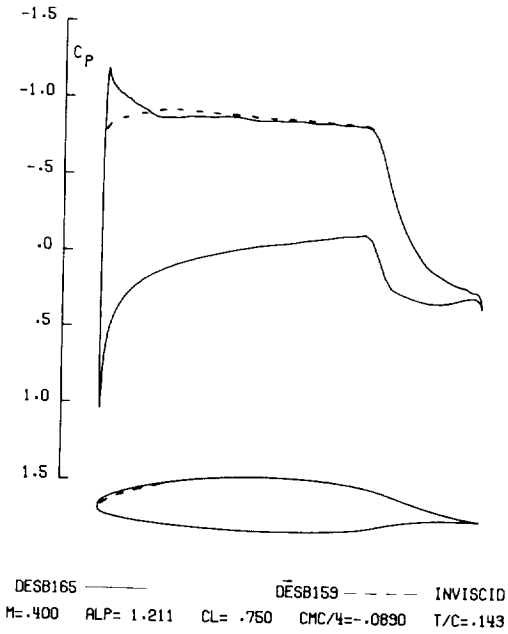

Figure 8.- Comparison of inviscid pressure distributions of DESB165 airfoil with the DESB159 airfoil at the climb condition.

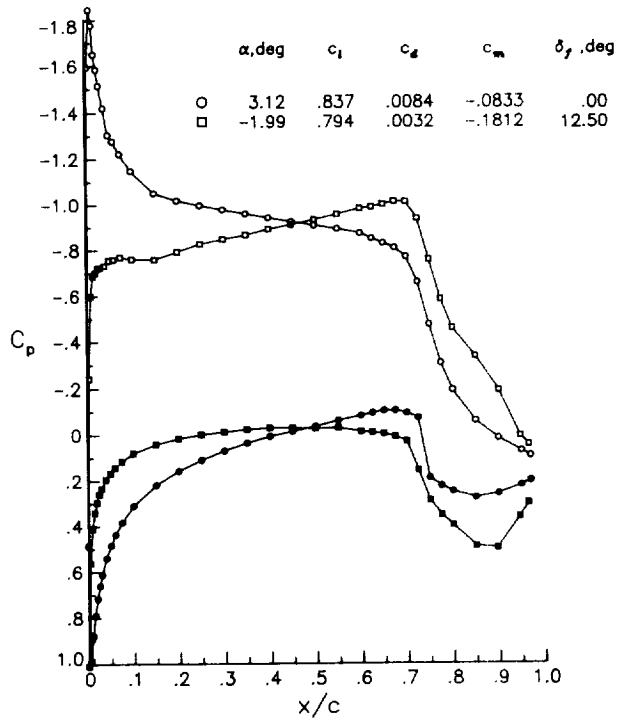

(a) Cruise flap deflection for low drag in climb.

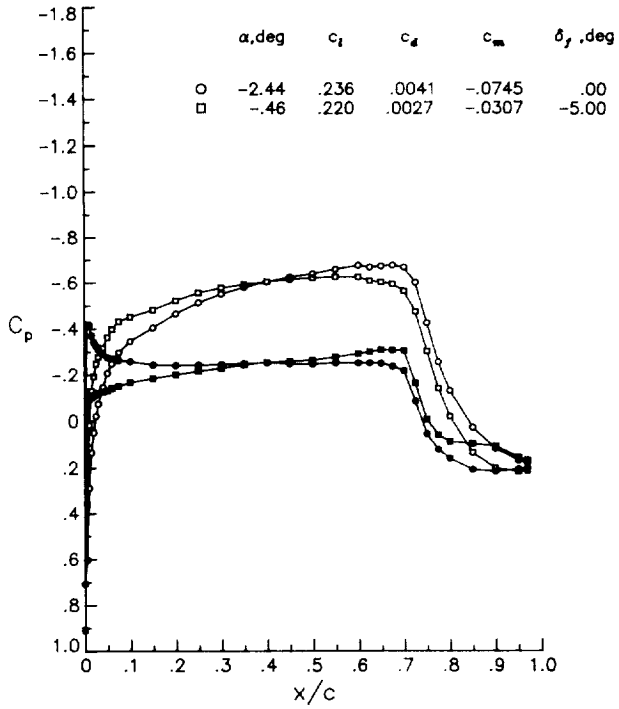

(b) Cruise flap deflection for low drag in cruise.

Figure 9.- Experimental pressure distributions on the NLF(1)-0414F airfoil at nearly constant section lift coefficients.

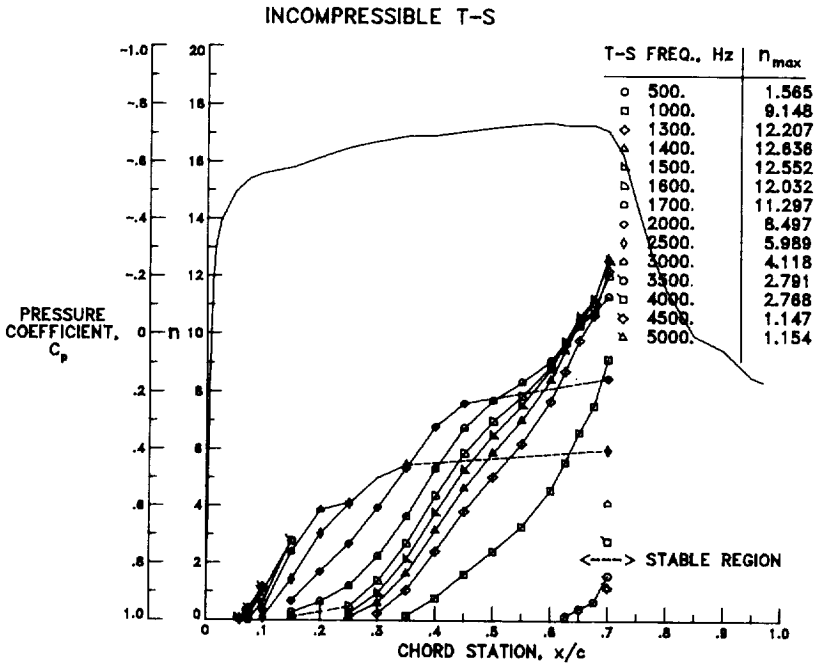

(a) Experimental pressure distribution and the incompressible amplification of various TS disturbance frequencies.

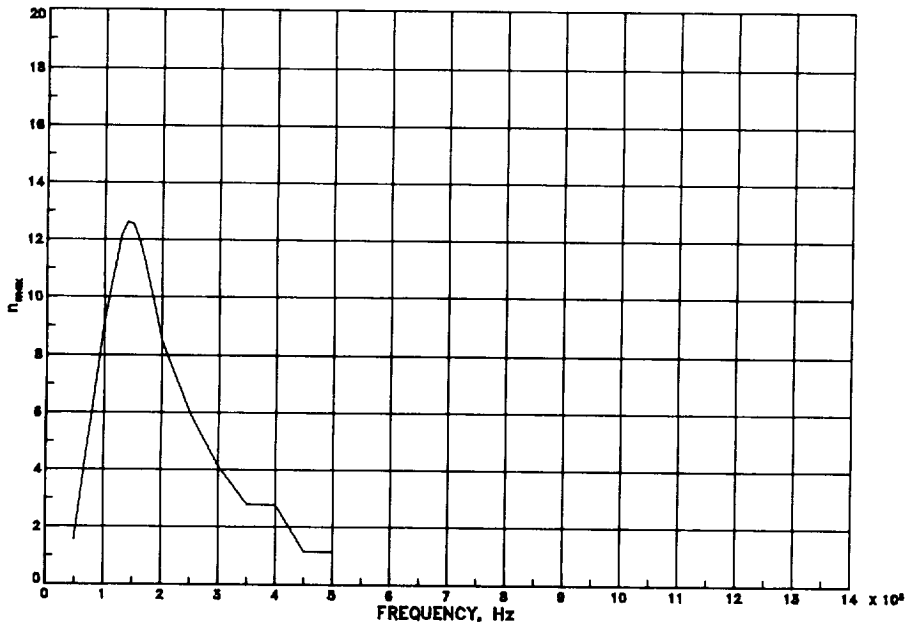

(b) Maximum incompressible logarithmic amplification versus TS disturbance frequency.

Figure 10.- Results of stability calculations at design conditions for the upper surface of NLF(1)-0414F.

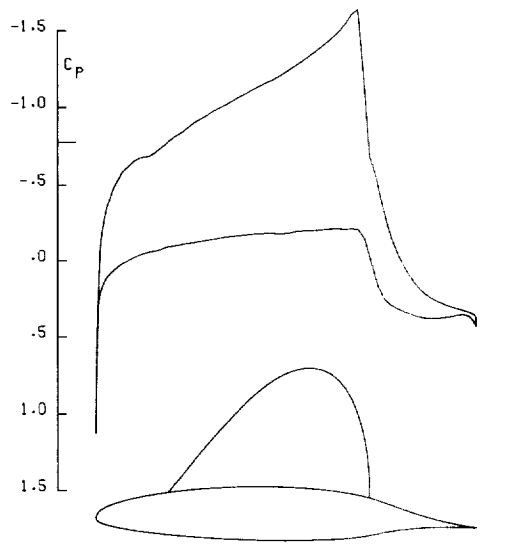

Figure 11.- Calculated inviscid pressure distribution of incompressible NLF(1)-0414F at compressible conditions.

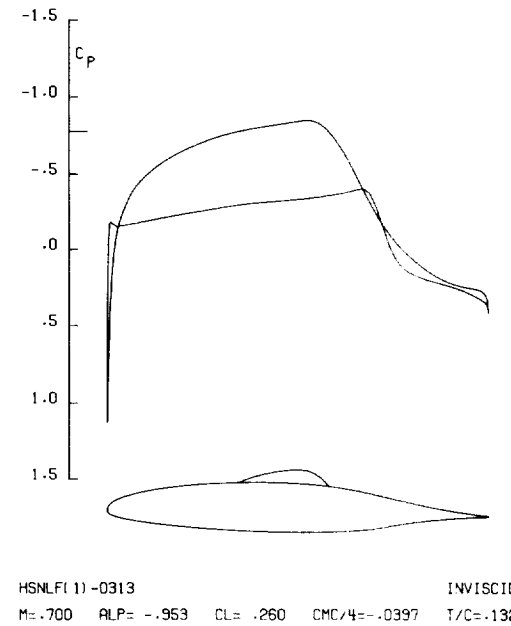

Figure 12.- Calculated inviscid pressure distribution of the flap de-cambered HSNLF(1)-0313 airfoil.

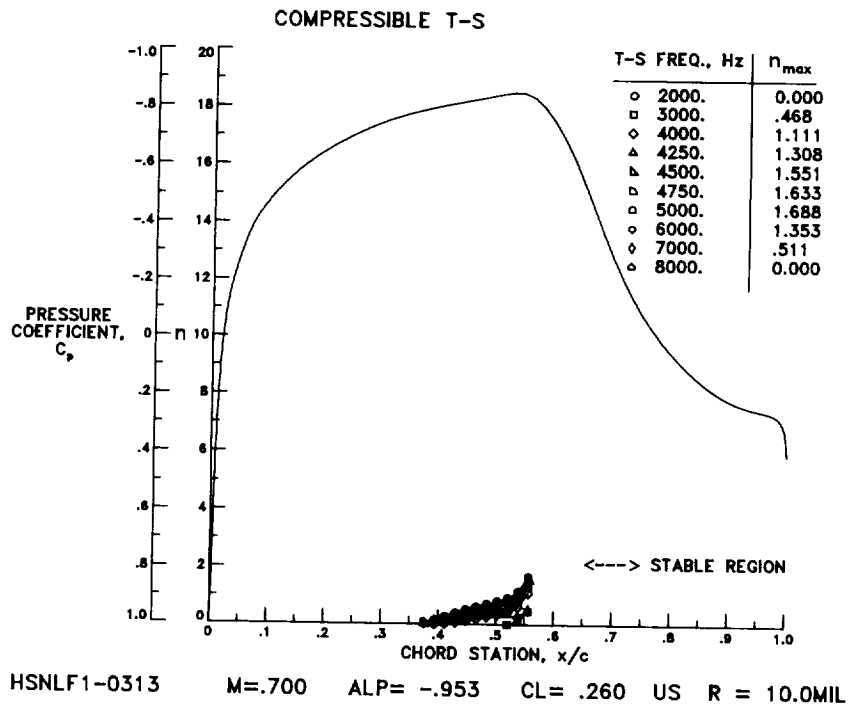

(a) Upper surface.

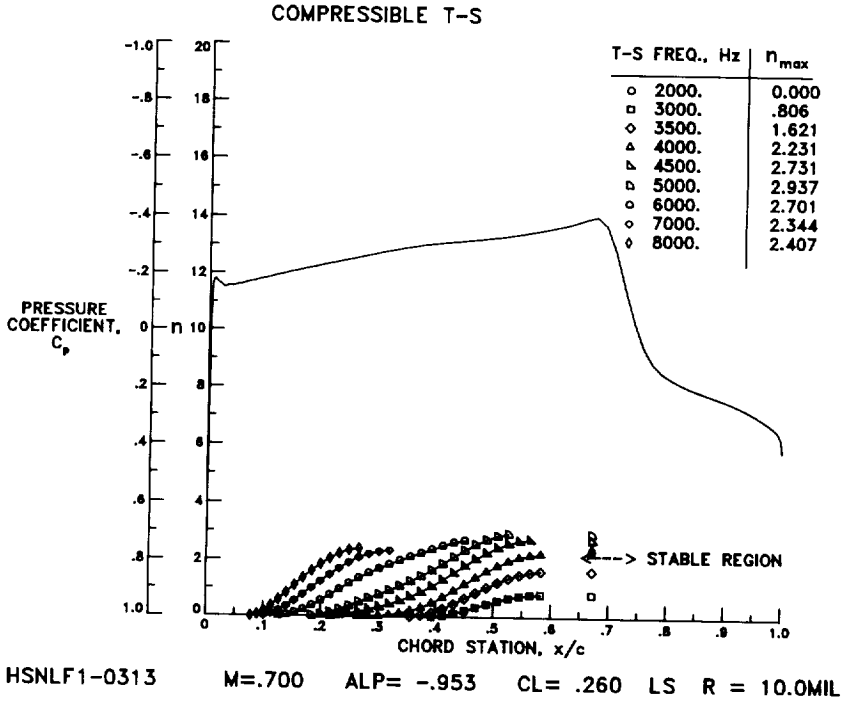

(b) Lower surface.

Figure 13.- Calculated pressure distribution and the compressible logarithmic amplification of various TS disturbance frequencies for HSNLF(1)-0313 at design.

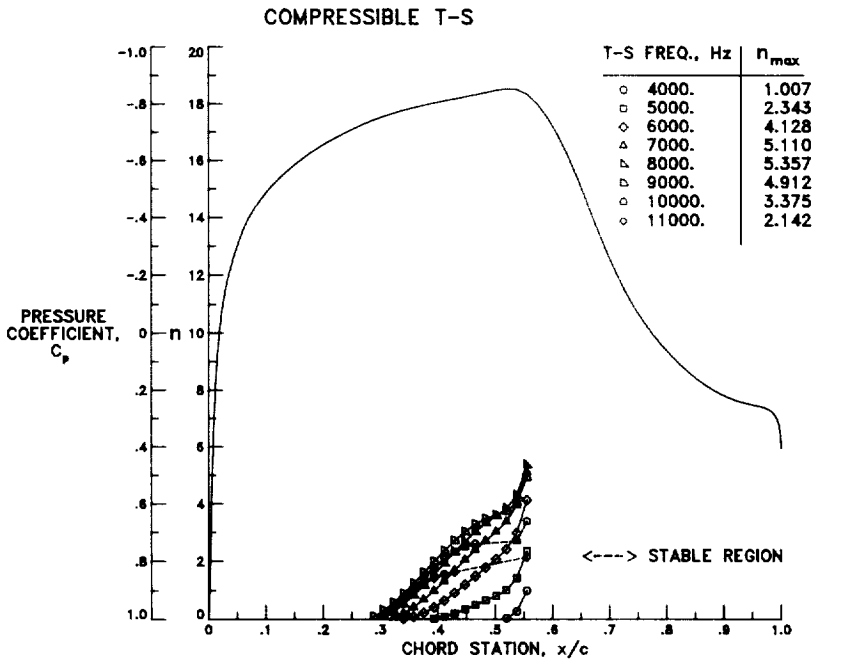

(a) Compressible logarithmic amplification.

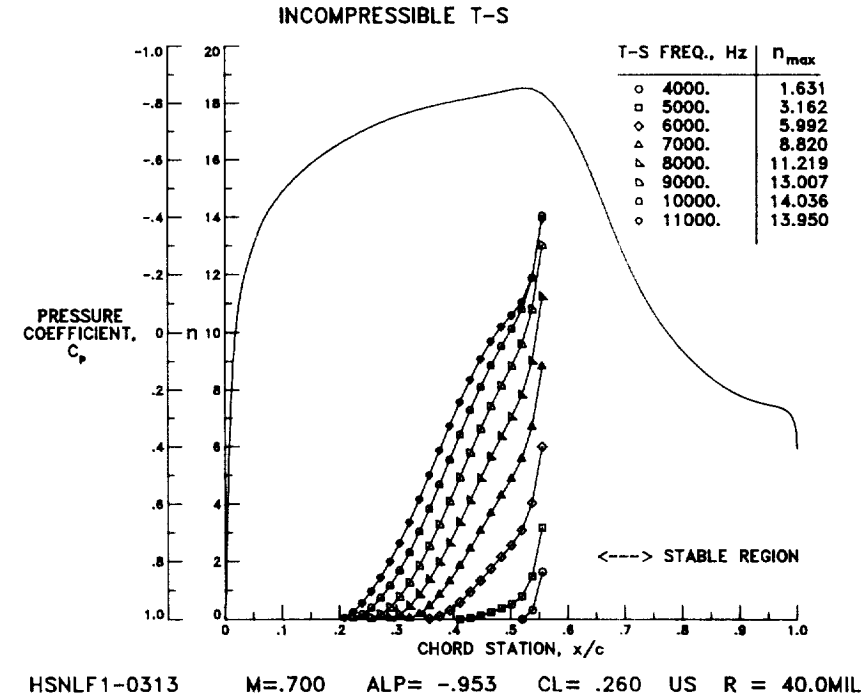

(b) Incompressible logarithmic amplification.

Figure 14.- Calculated pressure distribution and the logarithmic amplification of various TS disturbance frequencies for the upper surface of HSNLF(1)-0313 at $R = 40 \times 10^6$.

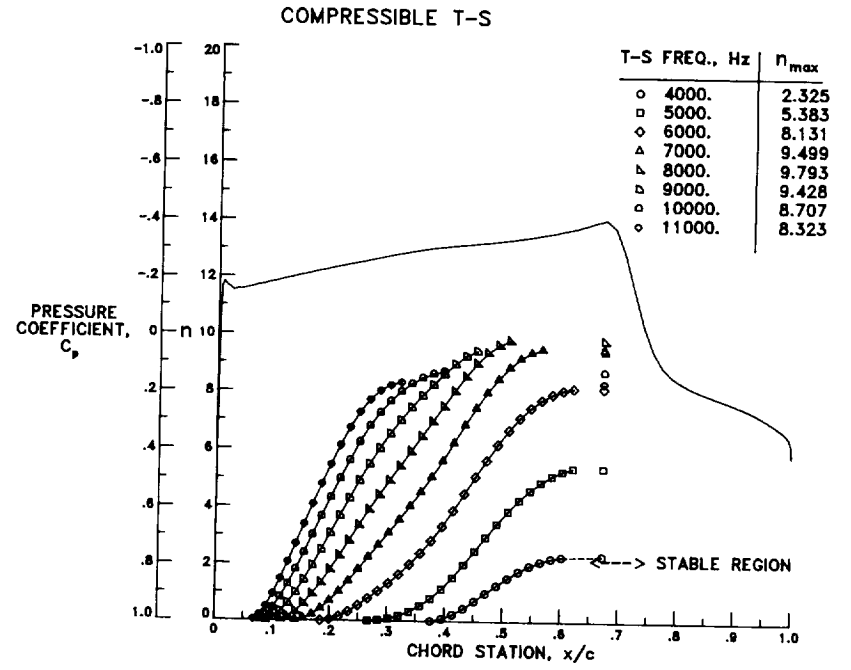

(a) Compressible logarithmic amplification.

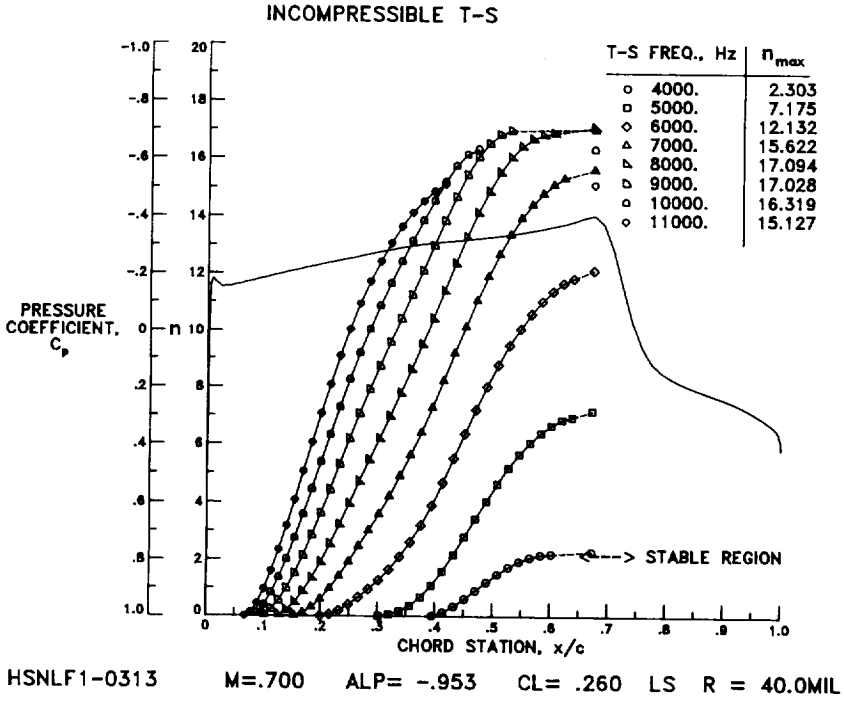

(b) Incompressible logarithmic amplification.

Figure 15.- Calculated pressure distribution and the logarithmic amplification of various TS disturbance frequencies for the lower surface of HSNLF(1)-0313 at $R = 40 \times 10^6$.

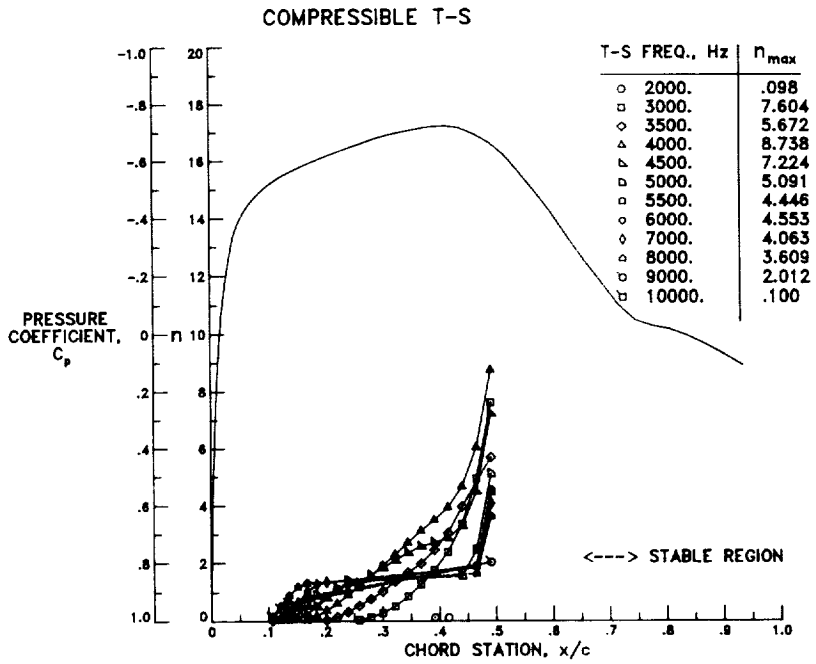

Figure 16.- Calculated three-dimensional pressure distribution and the compressible logarithmic amplification of various TS disturbance frequencies for the upper surface of the F-14 NASA glove.

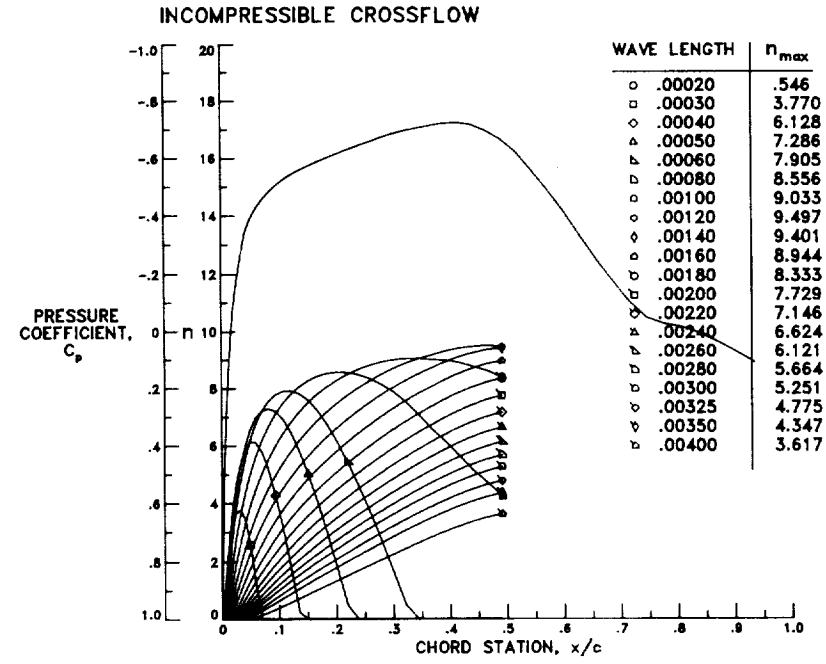

Figure 17.- Calculated three-dimensional pressure distribution and the incompressible logarithmic amplification of various crossflow disturbance wavelengths for the upper surface of the F-14 NASA glove.

ORIGINAL PAGE IS
OF POOR QUALITY

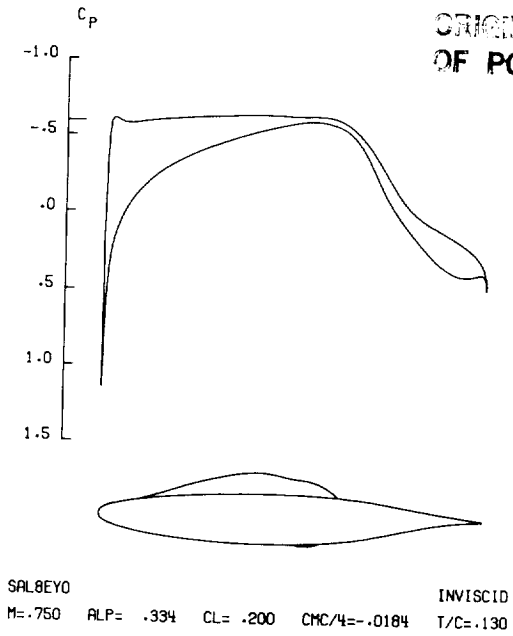

Figure 18.- Calculated inviscid pressure distribution of SAL8EY0 at the design case.

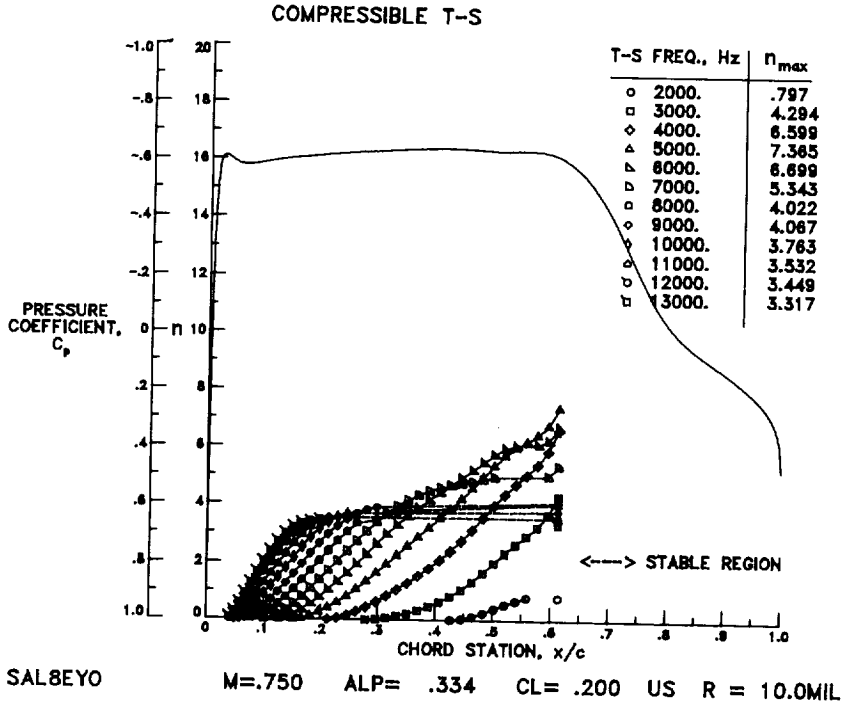

Figure 19.- Calculated inviscid pressure distribution and the compressible logarithmic amplification of various TS disturbance frequencies for the upper surface of the SAL8EY0 airfoil at design.

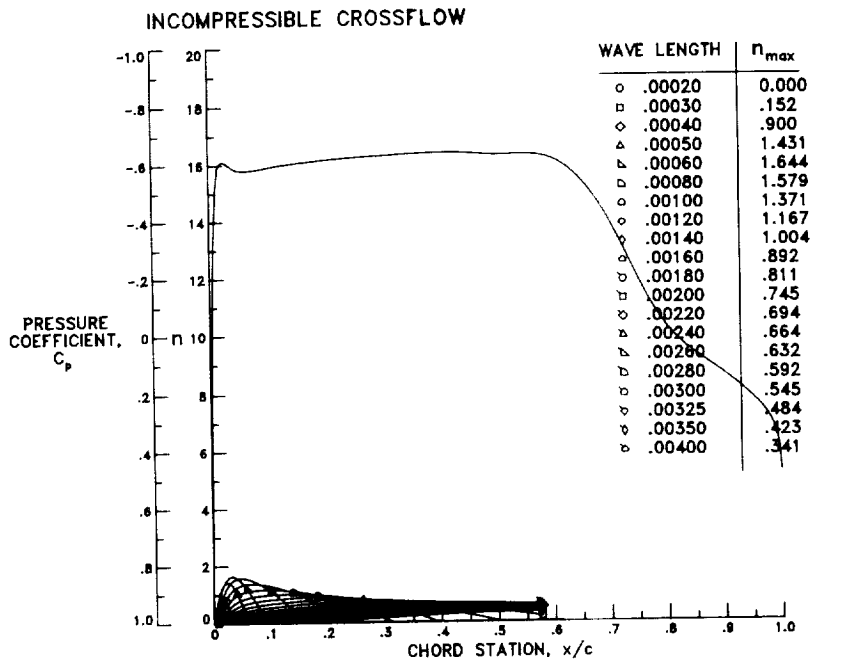

Figure 20.- Calculated inviscid pressure distribution and the incompressible logarithmic amplification of various crossflow disturbance wavelengths for the upper surface of the SAL8EYO airfoil at design.

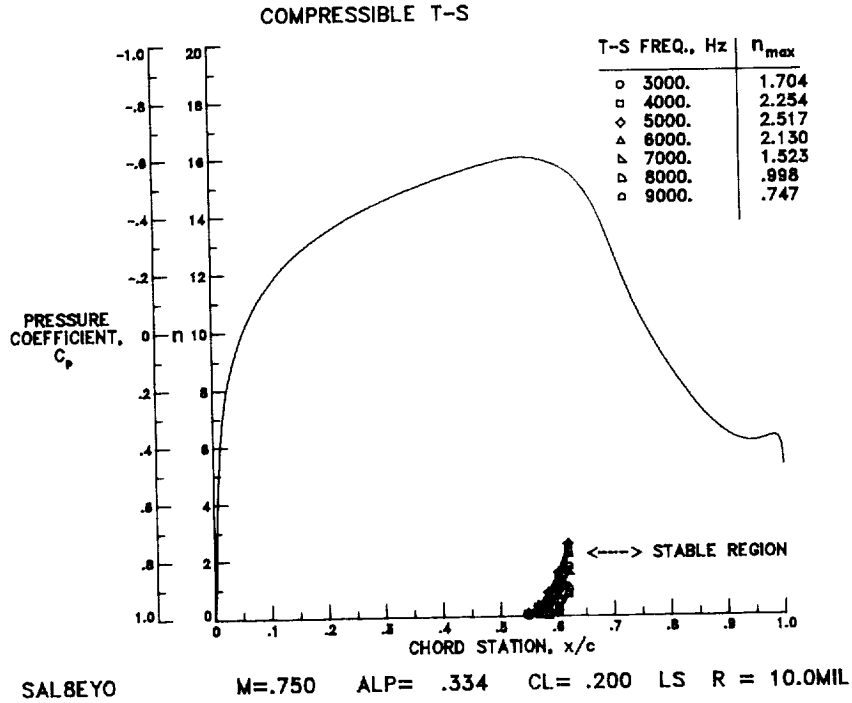

Figure 21.- Calculated inviscid pressure distribution and the compressible logarithmic amplification of various TS disturbance frequencies for the lower surface of the SAL8EYO airfoil at design.

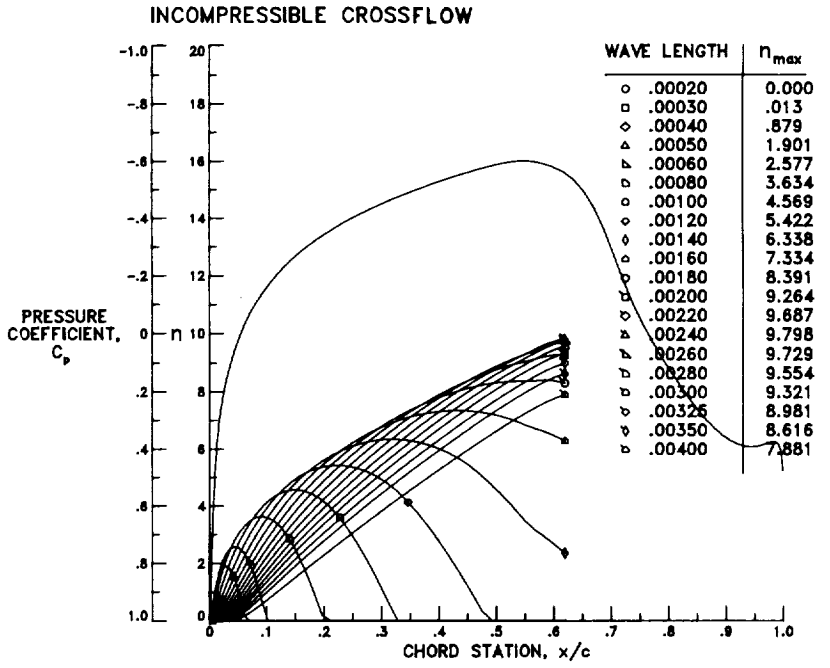

Figure 22.- Calculated inviscid pressure distribution and the incompressible logarithmic amplification of various crossflow disturbance wavelengths for the lower surface of the SAL8EYO airfoil at design.

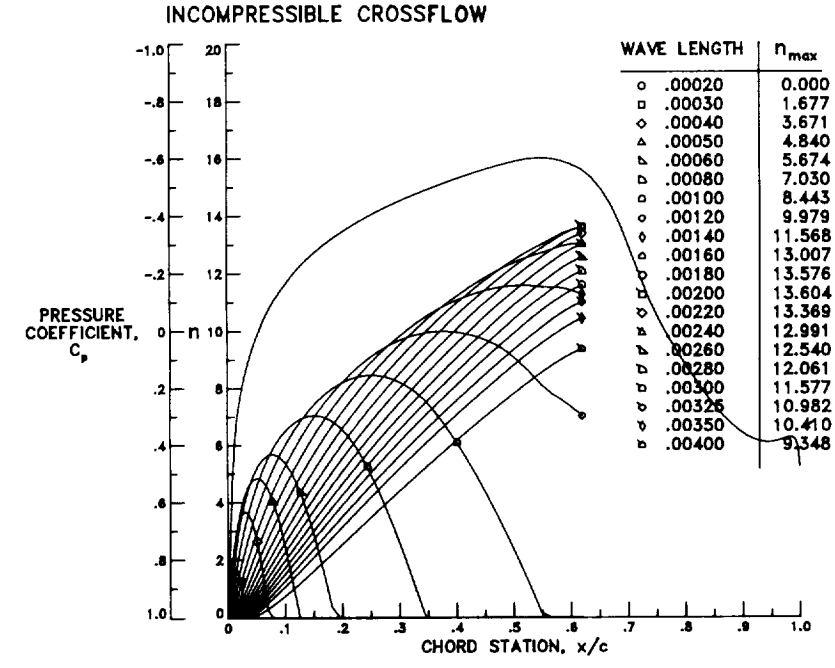

Figure 23.- Calculated inviscid pressure distribution and the incompressible logarithmic amplification of various crossflow disturbance wavelengths for the lower surface of the SAL8EYO airfoil at $R = 15.96 \times 10^6$.

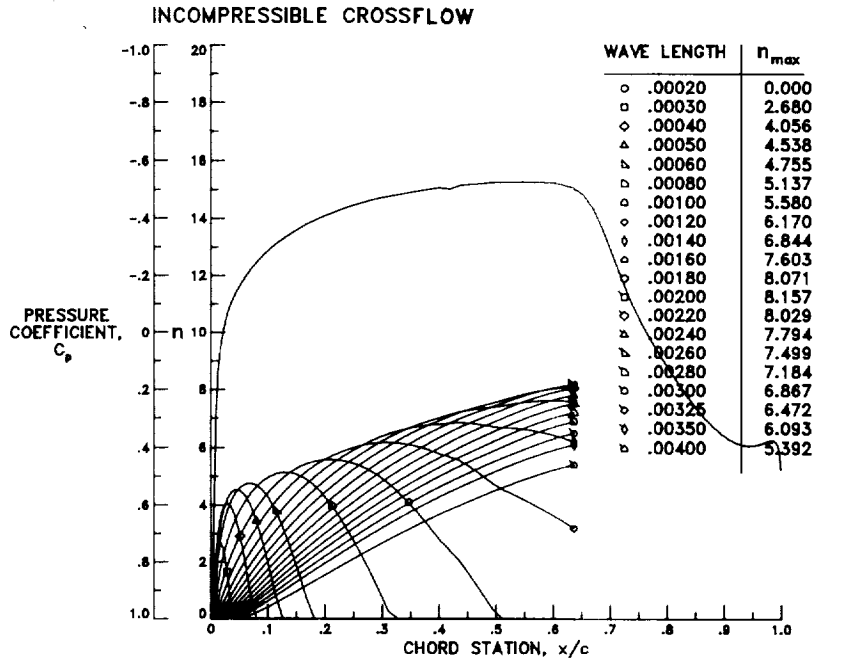

Figure 24.- Calculated inviscid pressure distribution and the incompressible logarithmic amplification of various crossflow disturbance wavelengths for the lower surface of CBLXF2 at $R = 15.96 \times 10^6$.

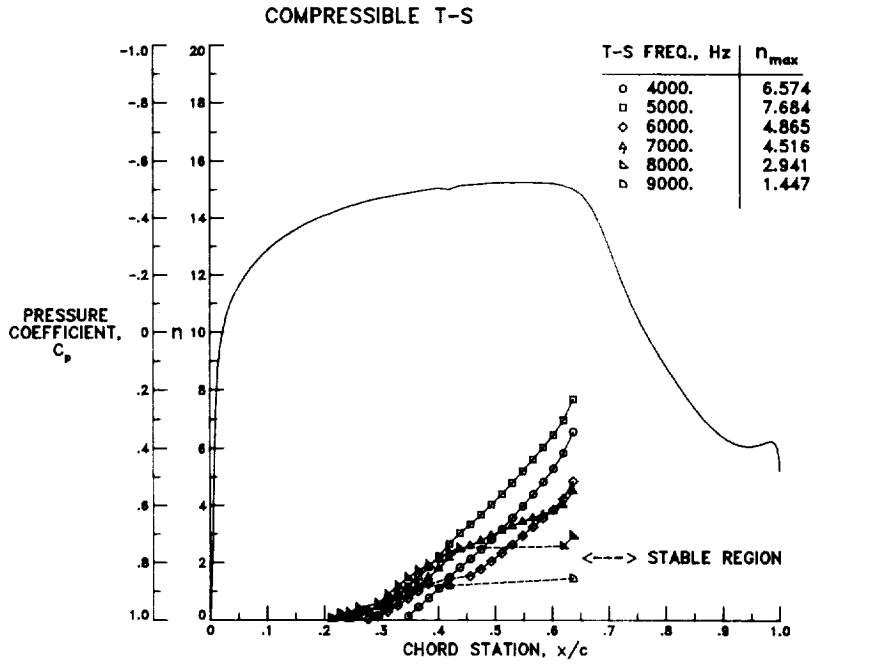

Figure 25.- Calculated inviscid pressure distribution and the compressible logarithmic amplification of various TS disturbance frequencies for the lower surface of CBLXF2 at $R = 15.96 \times 10^6$.